



Hydrotreatment of lipid model for diesel-like alkane using nitrogen-doped mesoporous carbon-supported molybdenum carbide

Fei Wang^a, Jianchun Jiang^{a,b,*}, Kui Wang^a, Qiaolong Zhai^a, Feng Long^a, Peng Liu^a, Junfeng Feng^a, Haihong Xia^a, Jun Ye^a, Jing Li^a, Junming Xu^{a,b}

^a Institute of Chemical Industry of Forest Products, Chinese Academy of Forestry, National Engineering Lab for Biomass Chemical Utilization, Key and Open Lab of Forest Chemical Engineering, SFA, Key Lab of Biomass Energy Sources and Materials, Nanjing 210042, China

^b Jiangsu Qianlin Biomass Energy Co., Ltd., Liyang 213364, China



ARTICLE INFO

Keywords:

Molybdenum carbide
Nitrogen-doped mesoporous carbon
Hydrotreatment
Vegetable oil
Polyaniline

ABSTRACT

The in situ polymerization of aniline as a nitrogen source was adopted to prepare nitrogen-doped mesoporous carbon (NMC), which further supported the molybdenum carbide catalyst for the hydrotreatment of fatty acids. The nitrogen doping drastically enhanced the catalytic performance of $\text{Mo}_2\text{C}/\text{N}_{1.0}\text{MC-700}$ with 92.7% conversion and 86.7% selectivity, which are much higher than the values of $\text{Mo}_2\text{C}/\text{MC}$ (84.8% and 70.1%, respectively). The kinetic study revealed that the apparent activation energy was reduced greatly after nitrogen doping. In addition, the nitrogen-doped catalyst showed decent stability, and the conversion and selectivity over $\text{Mo}_2\text{C}/\text{N}_{1.0}\text{MC-700}$ decreased by 4.4% and 6.9% respectively, after recycling three times. The deactivation mainly resulted from the coke deposition on the surface of catalyst. The high catalytic activity and stability were ascribed to the formation of pyridinic N and pyrrolic N in NMC, which resulted in the high dispersion of Mo, a decrease in the particle size as well as strong interactions between support and active sites. The hydrotreatment conditions of oleic acid were studied, and the optimal reaction conditions were as follows: reaction temperature, 350 °C; initial H_2 pressure, 3.0 MPa; n-hexane as solvent. Moreover, the results indicated that a substrate with a saturated carbon double bond and ester group was more easily converted into hydrocarbons.

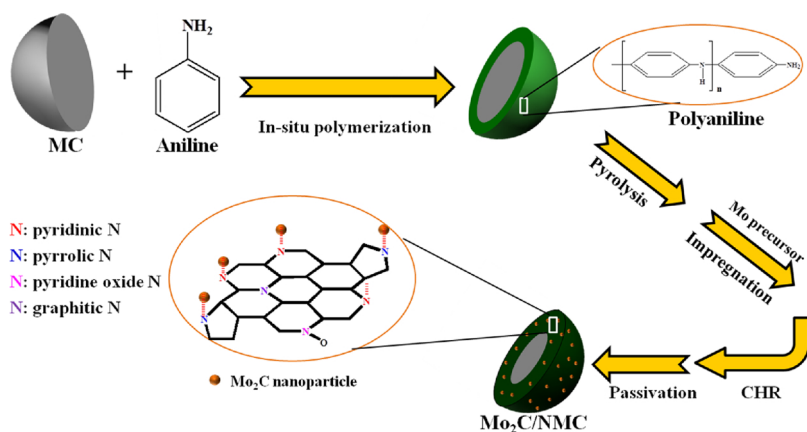
1. Introduction

Over the past several decades, we have witnessed the negative effects of abusing fossil fuels, i.e., environmental pollution and energy shortages. Therefore, renewable and sustainable energy, including solar, wind, hydro, nuclear, and bio-energy, has generated considerable research interest. Among these energy forms, bio-energy is the only type that can be used as a transportation fuel [1]. Triglycerides and fatty acids, which are the major components of oil and grease (including inedible vegetable oil and waste cooking oil), are regarded as a promising feedstock to produce bio-energy owing to their abundant carbon resources. Recently, fatty acid methyl ester (FAME), a first-generation bio-diesel, has replaced fossil diesel to some degree. Nevertheless, the application of FAME has drawbacks, such as high oxygen contents and poor cold-flow properties, which severely limit its further development [2].

Through catalytic hydrotreatment, triglycerides, fatty acids and fatty acid esters can be converted into a diesel-like alkane liquid, which is a potential substitute for fossil diesel because both have identical

chemical compositions [3]. The hydrotreatment reaction of triglycerides and FAME occurs in two main steps: 1) the formation of fatty acids by β -elimination or the formation of aldehydes by hydrolysis (for FAME) and 2) deoxygenation of the fatty acids and aldehydes by three reaction pathways, namely, decarboxylation (DCX), decarbonylation (DCN), and hydrodeoxygenation (HDO) [4]. Hydrotreatment of vegetable oil and its derivatives is commonly conducted over a noble metal [5–9] or sulfided molybdenum [10,11] because of their outstanding catalytic properties. Unfortunately, due to the expense of noble metal catalysts and environmental issues regarding sulfur usage in the preparation of sulfided molybdenum, researchers must reconsider the application of both catalysts [12]. In recent years, many studies have been conducted on transition metal carbides because of their excellent catalytic properties in deoxygenation reactions [13]. Relative studies have demonstrated that the Mo_2C catalyst shows a higher catalytic activity than Pt, Pd, MoS_2 and Ni catalysts for FAME hydrotreatment [14,15]. In our previous study, the catalytic performances of molybdenum carbide (Mo_2C) and tungsten carbide (W_2C) supported on a carbon material with different Mo loadings were compared and the results revealed that

* Corresponding author at: Institute of Chemical Industry of Forest Products, Chinese Academy of Forestry, Nanjing 210042, China.
E-mail address: bio-energy@163.com (J. Jiang).



Scheme 1. Schematic illustration of the preparation of the Mo₂C/NMC catalyst.

the activity of Mo₂C was much higher than that of W₂C [16]. However, an aggregation and excessive growth of Mo₂C particles always occur, and the stability of the catalyst for the hydrotreatment reaction is not ideal [14,17,18].

As a support, carbon materials offer many advantages, such as resistance to acidic and basic media, low cost and excellent thermal stability; however, weak interactions between the carbon support and metal particles easily results in aggregation or leaching of the metal particles [19–21]. Nitrogen doping is an effective way to modify carbon supports and improve catalytic activity because the addition of nitrogen to a carbon matrix changes the functional [22], chemical [23] and electrical properties of the matrix [24]. Dicyanamide, cyanamide and phenanthroline are commonly used as nitrogen sources to introduce nitrogen atoms into the carbon support [25,26]. In situ nitrogen doping into a carbon matrix using a chemical method achieves homogenous incorporation [27,28]. The use of nitrogen-doped carbon materials to support Pt [29], Pd [22,27], Ru [26], Ni [19], and Mo₂C catalysts [18] has been reported. Jing et al. prepared the N-doped molybdenum carbide with melamine as a nitrogen source for hydrogen evolution and the synergy between Mo₂C and the N dopants enhanced catalytic performance [18]. However, the application of a doped carbon-supported Mo₂C catalyst in the hydrotreatment of vegetable oil and its model compounds has not been reported so far.

Here, in situ aniline polymerization was used to prepare nitrogen-doped mesoporous carbon (NMC) as the support for molybdenum carbide. The nitrogen-doped catalyst was used for the hydrotreatment of model lipid compounds and the kinetics over Mo₂C supported on NMC and MC were compared. In addition, the functional and chemical properties of the catalysts were characterized. Moreover, the hydrotreatment conditions (parameters, solvent, and substrates), Mo loading as well as catalyst stability were investigated.

2. Experimental

2.1. Materials

Mesoporous carbon (MC, particle size: 125–180 μm), ammonium molybdate tetrahydrate, tetramethylammonium hydroxide (TMAH), n-eicosane, and platinum on carbon (Pt/C, 10 wt%) were purchased from Aladdin Co. Ltd. The hydrogen peroxide, dichloromethane, methanol, ammonium persulfate, aniline, melamine, nitric acid, perchloric acid, oleic acid, stearic acid, methyl oleate, methyl stearate, and n-hexane were provided by Sinopharm Chemical Reagent Co., Ltd. With the exception of aniline, all other chemicals were not purified before use. The oleic acid was composed of 11 wt% palmitic acid (C16:1) and 89 wt% oleic acid (C18:1).

2.2. Catalyst preparation

2.2.1. Preparation of the NMC

First, 30.0 g of MC was pretreated with 100 mL of H₂O₂ (30 wt%) under stirring at 50 °C for 5 h. Then, the solid was dried in a vacuum oven at 80 °C for 12 h. Next, 0.5, 1.0 or 1.5 g of aniline was dissolved in 36 mL of an HCl solution (1.0 mol·L^{−1}) and homogeneously mixed with 5.0 g of pretreated MC to obtain mixture A. Then, 2.5 g of ammonium persulfate was dissolved in 13 mL of a HCl solution (1.0 mol·L^{−1}) to obtain mixture B. Mixture B was added dropwise into mixture A under magnetic stirring at 0 °C, and the polymerization reaction lasted 3 h. Afterwards, the solid was washed successively with 100 mL of a HCl solution (1.0 mol·L^{−1}) and 100 mL of a NH₄OH solution (1.0 mol·L^{−1}). After washing with distilled water three times, the sample was dried overnight at 80 °C under a vacuum. Finally, polyaniline-coated MC was annealed in a tube furnace under N₂ with a heating rate of 5 °C min^{−1} to the pyrolysis temperature (700 °C, 800 °C, or 900 °C) for 2 h. The obtained samples were designated N_xMC-T (where x represents the aniline amount 0.5, 1.0 or 1.5 and T represents the pyrolysis temperature 700, 800, or 900). For comparison, the nitrogen sources, melamine or aniline (without polymerization) were also introduced into the MC by a direct impregnation method, respectively.

2.2.2. Preparation of the Mo₂C/NMC catalyst

Mo₂C supported on NMC was synthesized using the carbothermal hydrogen reduction (CHR) method described in previous studies with some modifications [14,30]. First, the molybdenum precursor was introduced into 4.0 g of NMC by an incipient wetness impregnation method under ultrasonic assistance for 1 h. Subsequently, the obtained sample was dried at 80 °C in a vacuum oven for 12 h. In addition, carburization was carried out in a tube furnace under a H₂ flow with the following temperature ramp: from ambient temperature to 450 °C at 5 °C min^{−1}, and then to 700 °C at 1 °C min^{−1} and held for 2 h. Finally, the catalyst was passivated in a flow of 1% O₂/N₂ at ambient temperature for 2 h. The schematic illustration of the preparation of the Mo₂C/NMC catalyst is shown in **Scheme 1**.

2.3. Catalyst characterization

X-ray diffraction (XRD) was used to identify the crystalline phases of the catalysts. The XRD spectra were recorded on a D8 Focus diffractometer at a rate of 10.0° per minute in the range $2\theta = 10.0\text{--}80.0^\circ$ using Cu K_α radiation at 40 kV.

X-ray photoelectron spectroscopy (XPS) was performed on a Thermo Fisher Escalab 250xi. The spectra were collected using an aluminum anode (Al K_α = 1486.6 eV) at 14.8 kV and 4.5 mA with an analyzer pass energy of 100 eV for wide scans and 30 eV for narrow scans. The energy correction was based on the C 1s peak of adventitious carbon at

284.5 eV. The XPS patterns were fitted using Advantage software.

Transmission electron microscopy (TEM) images were obtained using a Fei Tecnai G2 operated at 200 kV. The catalyst sample was first ground and suspended in ethanol. After ultrasonic treatment the suspension was dropped onto a copper grid coated with a carbon film. The particle size distribution was calculated by measuring the size of more than 200 random particles in the TEM images.

Scanning electron microscope (SEM) images were generated using a Hitachi 3400-I operated at 15 kV to observe the morphologies of the catalyst. The samples were covered by a thin gold film for enhanced image definition. The Mo identification and relative distribution were mapped by energy dispersive spectroscopy (EDS) on a Horiba EMAX instrument coupled with SEM.

The textural parameters of the catalysts were analyzed by N_2 sorption isotherms with a Micrometric ASAP 2020 at -196°C . Prior to the measurement, the catalyst was degassed under a vacuum at 200°C for 10 h. The BET surface area was calculated from the linear portion of the BET plot method.

H_2 temperature programmed reduction (H_2 -TPR) was performed using a Quantachrome ChemBET Pulsar TPR/TPD instrument equipped with a thermal conductivity detector (TCD). Approximately 0.05 g of sample was first dried at 300°C for 1 h in 50 mL min^{-1} He. Subsequently, the sample was cooled to 40°C , and He was changed to 75 mL min^{-1} H_2/Ar . Finally, when the TCD signal was stable, the reduction was conducted at a heating rate of $10^\circ\text{C min}^{-1}$ to 800°C in 75 mL min^{-1} H_2/Ar . The hydrogen consumption was determined by the TCD. Before detection, the gas was passed through a cold trap filled with a mixture of liquid nitrogen and acetone to remove the resulting water.

The number of active sites in the catalysts was measured using CO chemical adsorption on an AutoChem II 2920 instrument. Approximately 200 mg of sample was pretreated in flowing 30 mL min^{-1} 10% H_2/Ar at 700°C for 1 h. Then, the sample was cooled down to 50°C in a 30 mL min^{-1} He flow. Once the baseline stabilized, 10% CO/He was injected several times until the surface of the sample was saturated with CO. The exposed molybdenum sites on the surface were estimated from the quantity of CO chemisorption with a stoichiometry of 1:1 [31,32].

The nitrogen content of the NMC support was determined using a Thermo Fisher 2000 elemental analyzer. The amount of Mo in the catalysts was identified by inductively coupled plasma-optical emission spectroscopy (ICP-OES) on a PerkinElmer Optima 7000 instrument after pretreatment with nitric acid and perchloric acid.

2.4. Hydrotreatment reaction

Hydrotreatment of model triglycerides was performed in a 250-mL batch reactor with electric heating. First, 10.0 g of the substrate, 50.0 g of n-hexane solvent and 1.0 g of catalyst were added into the reactor. Then, the reactor was purged with H_2 three times and pressurized to 3.0 MPa. Subsequently, the batch reactor was heated to 350°C and held for 3 h. The mixture in the reactor was stirred mechanically at 500 rpm during the reaction. When the reactor cooled to ambient temperature, the liquid product was collected. During the catalyst recycling study, the feedstock and the solvent were immediately added once the liquid product was taken out of the reactor. In the kinetic experiments, the independent hydrotreatment of stearic acid was conducted to study the effects of the particle size of the catalysts (180–250, 125–180 and 75–125 μm) and the agitation speed of the reactor (400, 500, 700 and 1000 rpm). The variation in the conversion of stearic acids as particle size and agitation speed changed were negligible. Therefore, the kinetic experiments (particle size of catalysts: 125–180 μm ; agitation speed: 500 rpm) can be considered free from the limitation of diffusion.

The chemical composition of the liquid products was identified by gas chromatography (GC) (Agilent 7890 A/5975C). First, 0.2 μL of the samples was injected into the instrument. The capillary

chromatographic column was a HP-5MS ($30\text{ m} \times 0.25\text{ mm} \times 0.25\text{ }\mu\text{m}$); the temperature of the injector was 260°C , and the split ratio of the carrier gas was 1:50. The carrying gas was high-purity helium. The oven temperature program proceeded as follows: first, the temperature was held at 150°C for 2 min; then, the temperature was increased from 150°C to 280°C at a rate of $10^\circ\text{C min}^{-1}$ and held at 280°C for 10 min. For the MS conditions, the ionization parameters were as follows: ionization methods, EI; ionization energy, 70 eV; scan per second over the electron range (m/z), 30–500 amu; ion source temperature, 230°C . N-eicosane was used as the internal standard for accurate quantification. For chemical composition analysis, 0.5 g of the sample was first dissolved in a mixture of $\text{CH}_2\text{Cl}_2/\text{MeOH}$ (2:1), which was then methylated with TMAH to eliminate fatty acids.

The conversion of the substrate is defined by the following equation:

Conversion = $(C_F - C_O)/C_F \times 100\%$ where C_F and C_O are the carbon moles of initial feedstock and the oxygenates in the product, respectively.

The selectivity of hydrocarbons in the liquid product is given by:

Selectivity = $C_{HC}/C_P \times 100\%$ where C_{HC} and C_P are the carbon moles of hydrocarbons in the product and carbon moles of total product, respectively.

The cracking ratio is calculated by:

Cracking ratio = $C_{LC}/C_P \times 100\%$ where C_{LC} and C_P are the carbon moles of light hydrocarbons (carbon number from 9 to 14) in the product and carbon moles of total product, respectively.

The HDO/DC ratio of hydrodeoxygenation versus decarboxylation plus decarbonylation is calculated by:

HDO/DC ratio = $(C_{16} + C_{18})/(C_{15} + C_{17}) \times 100\%$ where C_{16} , C_{18} , C_{15} and C_{17} are the relative carbon moles of hexadecane, octadecane, pentadecane, and heptadecane, respectively.

3. Results and discussion

3.1. Characterization of the catalysts

Fig. 1 exhibits the XRD spectra of the pretreated MC, $\text{Mo}_2\text{C}/\text{MC}$, $\text{Mo}_2\text{C}/\text{N}_{0.5}\text{MC}-800$, and $\text{Mo}_2\text{C}/\text{N}_{1.0}\text{MC}-800$ catalysts. The broad peaks at 24° and 44° in the pattern of pretreated MC can be attributed to the (002) plane of the graphite structure and the (100) plane of interlayer condensation, respectively [33]. However, after CHR both peaks totally disappeared as shown in the $\text{Mo}_2\text{C}/\text{MC}$ spectrum, while the peaks remained in the spectra of $\text{Mo}_2\text{C}/\text{N}_{0.5}\text{MC}-800$ and $\text{Mo}_2\text{C}/\text{N}_{1.0}\text{MC}-800$, which indicated that nitrogen doping promoted the formation of a graphitic network [34]. After CHR, diffraction peaks appeared at 34.4° ,

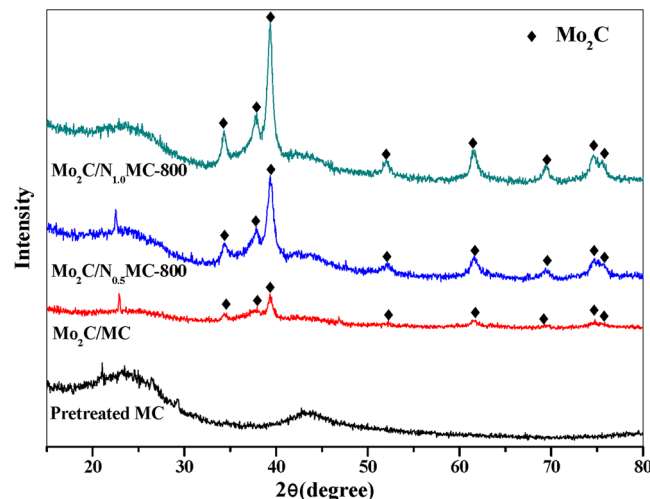


Fig. 1. XRD spectra of pretreated MC, $\text{Mo}_2\text{C}/\text{MC}$, $\text{Mo}_2\text{C}/\text{N}_{0.5}\text{MC}-800$, and $\text{Mo}_2\text{C}/\text{N}_{1.0}\text{MC}-800$ catalysts.

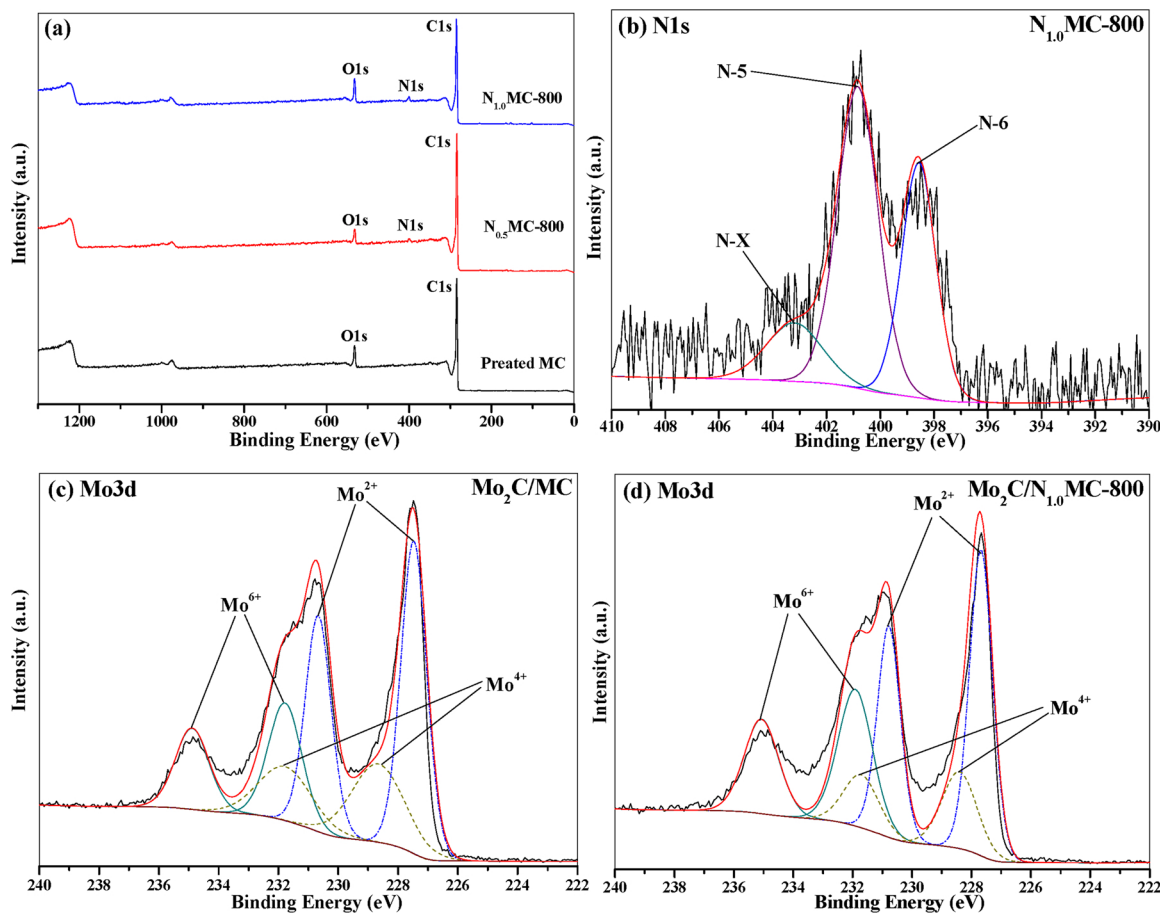


Fig. 2. XPS survey patterns of the supports (a); N1 s XPS spectra (b) of N_{1.0}MC-800; Mo3d XPS spectra of the Mo₂C/MC (c) and Mo₂C/N_{1.0}MC-800 (d).

38.0°, 39.4°, 52.1°, 61.5°, 69.6°, 74.6°, and 75.5°, which were assigned to the (100), (002), (101), (102), (110), (103), (112), and (201) planes of Mo₂C (JCPDS 35-0787), respectively [31,35,36]. Moreover, with an increase in the nitrogen content the diffraction peaks became more distinct.

The XPS patterns were obtained to analyze the elemental composition (C, N, and Mo) and valence states of the elements on the supports/catalysts. The N 1 s and Mo 3d XPS spectra and corresponding quantitative analysis are shown in Figs. 2 and S1 (Supplementary information) and Table 1. In addition, the nitrogen content identified by elemental analysis is also listed in Table 1. Elemental analysis proved that 0.70 wt% nitrogen existed in the pretreated MC, but traces of nitrogen were hardly detected by XPS. The survey XPS patterns of

N_{0.5}MC-800 and N_{1.0}MC-800 in Fig. 2(a) revealed that nitrogen was successfully doped into the MC as indicated by the presence of the peak at 400 eV. In addition, the peak became more intense as aniline usage increased, as evidence of the improved nitrogen content. The elemental analysis in Table 1 confirms that the nitrogen content increased from 0.70 wt% to 1.84 wt% and 2.17 wt%. High-resolution N 1 s spectroscopy further displayed the presence of three types of nitrogen atoms: pyridinic N (N-6 at 398.4 eV), pyrrolic N (N-5 at 400.3 eV) and pyridine N-oxide (N-X at 402.7 eV) [26,37–39]. Figs. 2(b) and S1(a) show that graphitic N (N-Q) did not form [22,24,40–42] and might combine with N-X, according to the research by Pels [43]. Reportedly, N-5 and N-6 in the support play a dominant role in anchoring active sites and enhancing their dispersion [44]. In addition, due to lone-pair electrons serving as metal coordination sites, N-5 and N-6 can stabilize active sites [45]. Therefore, improving the proportion of N-5 and N-6 is desired. Herein the proportion of N-6 and N-5 in N_{0.5}MC-800 and N_{1.0}MC-800 was 76.5% and 86.1%, respectively, which is higher than that in the nitrogen-doped mesoporous carbon (only 50%) using melamine as a nitrogen source [29].

Figs. 2(c), (d), and S1(b) exhibit the high-resolution Mo 3d XPS patterns. The fitting method was the same as that used in our previous research [14]. Mo existed in three valence states in the Mo₂C/MC, Mo₂C/N_{0.5}MC-800, and Mo₂C/N_{1.0}MC-800 catalysts: 227.7 eV (Mo-3d_{5/2}) and 230.9 eV (Mo-3d_{3/2}), corresponding to Mo(II) in Mo₂C; 228.8 eV (Mo-3d_{5/2}) and 232.0 eV (Mo-3d_{3/2}) for Mo (IV) in MoO₂; 231.7 eV (Mo-3d_{5/2}) and 234.9 eV (Mo-3d_{3/2}) for Mo (VI) in MoO₃. The doped nitrogen had little influence on the Mo₂C percentage but influenced MoO₂ and MoO₃, as listed in Table 1, which indicated that nitrogen in the carbon skeleton promoted the formation of MoO₃ and inhibited the formation of MoO₂. However, the variation in the

Table 1
Relative quantitative analysis of N and Mo with XPS.

Catalyst	N content ^a (wt%)	N 1s ^b			Mo 3d ^c		
		N-6(%)	N-5(%)	N-X(%)	II(%)	IV(%)	VI(%)
Mo ₂ C/MC	0.70	0.0	0.0	0.0	49.8	25.8	24.4
Mo ₂ C/ N _{0.5} MC- 800	1.84	36.0	40.5	23.5	50.4	13.2	36.4
Mo ₂ C/ N _{1.0} MC- 800	2.17	34.1	52.0	13.9	48.8	18.7	32.5

^a Determined by elemental analysis of pretreated MC and NMC-800.

^b Identified by XPS analysis on NMC-800; N proportion based on the fitted peak areas.

^c Detected by XPS analysis on catalysts; Mo proportion based on the fitted peak areas.

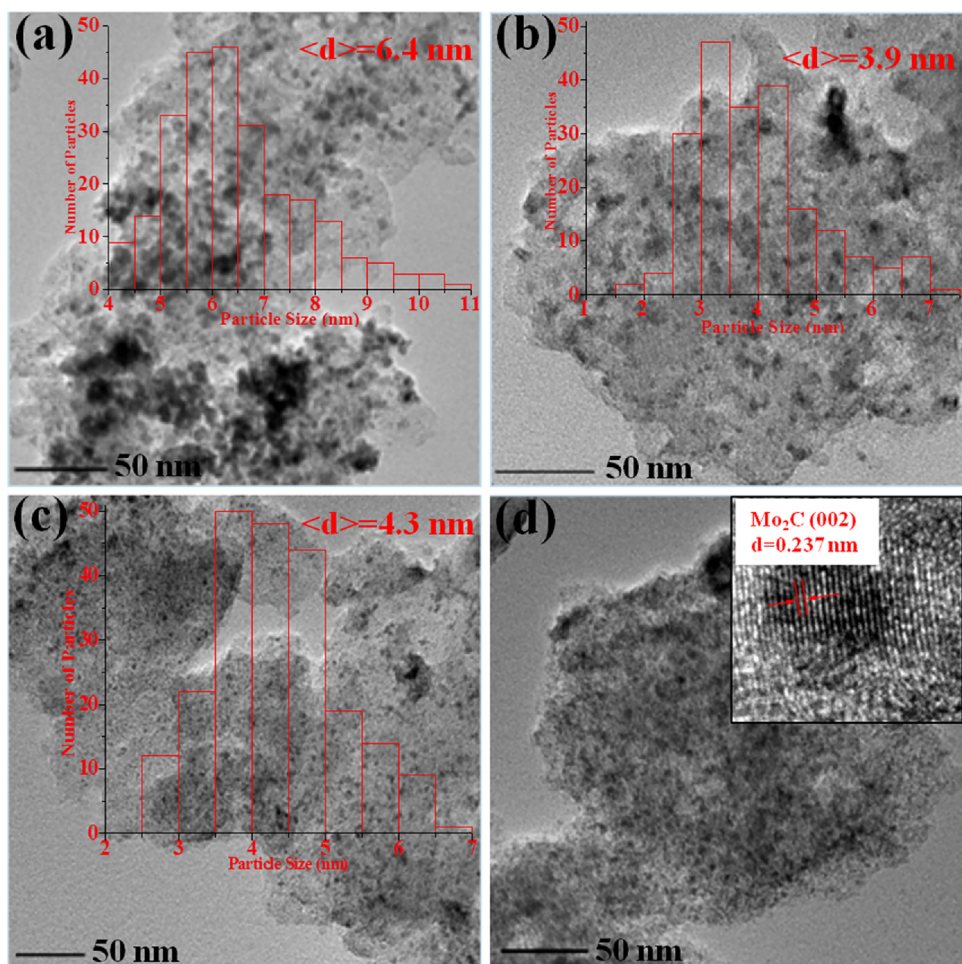


Fig. 3. TEM images of Mo₂C/MC (a), Mo₂C/N_{1.0}MC-800 (b) and Mo₂C/N_{0.5}MC-800 (c and d). The insets in a, b, and c show the particle size distribution of the active sites and the insets in d is the HR-TEM image.

proportion of MoO₂ and MoO₃ had a minimal effect on the activity because the main active sites were Mo₂C with a high catalytic activity.

To obtain more details about the morphology and nanoparticle distribution of the catalysts, the TEM and SEM images were analyzed. The TEM images show that serious agglomeration of Mo₂C particles occurred on the Mo₂C/MC catalyst, as exhibited in Fig. 3(a). In contrast, nitrogen doping clearly resulted in the uniform dispersion of Mo₂C nanoparticles on the surface of NMC-800. The average particle size was measured from the TEM images, and the results are listed in Table 2. As expected, the particle size decreased greatly from 6.4 nm to 4.3 nm and 3.9 nm with the increase in nitrogen doping. High-resolution TEM images showed Mo₂C nanoparticles with excellent crystallinity and a

distinct lattice spacing of 0.237 nm, confirming the (002) plane of Mo₂C. Well-dispersed nanoparticles with smaller sizes resulting from nitrogen doping in carbon materials have been reported before on Cu, Ni and Pd catalysts [19,22,46]. The CO chemical adsorption analysis in Table 2 corresponds to the TEM results. After nitrogen doping, the CO quantity increased from 7.98 μmol/g_{cat} to 17.26 and 23.16 μmol/g_{cat}, and the dispersion of Mo improved from 0.37% to 0.52 and 0.90%. In order to verify whether the change of textural properties after nitrogen doping contributed to uniform dispersion and reduced particle size of active sites, the N₂-sorption of pretreated MC, N_{0.5}MC-800 and N_{1.0}MC-800 were conducted (Table 2). The results revealed that after nitrogen doping the surface area and total pore volume of N_{0.5}MC-800 and

Table 2
Textural properties of the support and catalysts and the size of the nanoparticles.

Sample	CO quantity ^a (μmol/g _{cat})	Dispersion ^a (%)	Particle size ^b (nm)	S _{BET} ^c (m ² ·g ⁻¹)	D _{BHJ} ^c (nm)	V ^c (cm ³ ·g ⁻¹)
MC	–	–	–	768	4.3	0.46
Pretreated MC	–	–	–	786	4.3	0.48
N _{0.5} MC-800	–	–	–	534	4.4	0.34
N _{1.0} MC-800	–	–	–	454	3.8	0.27
Mo ₂ C/MC	7.98	0.37	6.4 ± 1.3	518	4.2	0.33
Mo ₂ C/N _{0.5} MC-800	17.26	0.52	4.3 ± 0.8	387	4.2	0.23
Mo ₂ C/N _{1.0} MC-800	23.16	0.90	3.9 ± 1.1	379	4.4	0.26

^a Detected by CO chemical adsorption.

^b Measured by TEM images (more than 200 particles).

^c Identified by N₂ sorption.

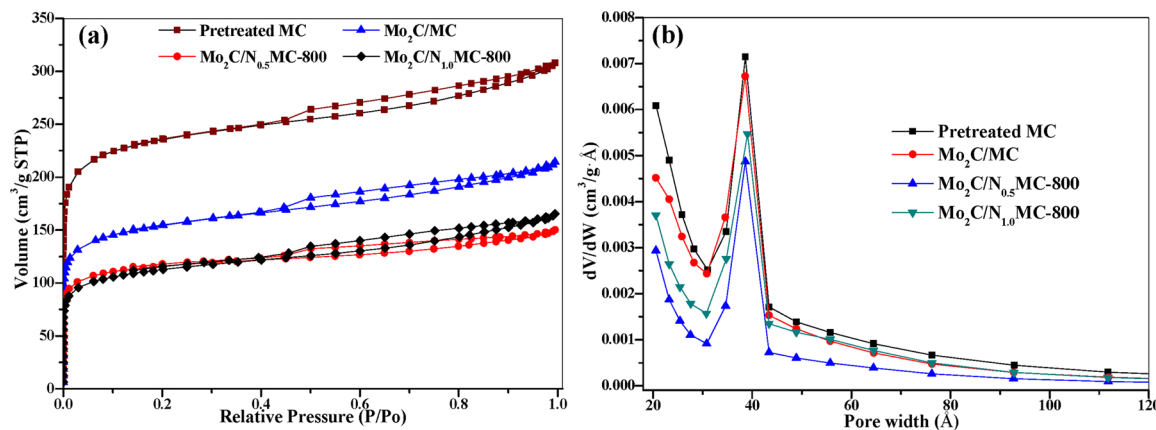


Fig. 4. Nitrogen sorption isotherms (a) and pore size distribution (b) of pretreated MC and catalysts.

$\text{N}_{1.0}\text{MC-800}$ decreased drastically. This indicated that the increased dispersion and the reduced particle size of active sites were not caused by the improvement of the textural properties after nitrogen doping. The commonly accepted explanations are that nitrogen contributes to the nucleation and growth of the nanoparticles [47] or alters the local electronic structure of the carbon support, allowing preferential growth of the nanoparticles [48].

The SEM images in Fig. S2 (Supplementary information) revealed that the surface of MC was smooth and few pores were found. Interestingly, many pores were densely scattered on the surface of NMC-800, as shown in Fig. S2(b) and (c). The in situ polymerization of aniline occurred on the surface of MC and further pyrolysis at 800 °C restructured the appearance. A rough surface can enhance the dispersion of metals as well as the interaction between the support and active sites. The EDS elemental mapping in the inset of Fig. S2(b) clearly exhibited the distribution of Mo, indicating that Mo was successfully loaded on NMC-800.

The N_2 -sorption isotherms and pore size distribution of the pretreated MC and catalysts are displayed in Fig. 4. In addition, the corresponding textural properties are listed in Table 2. As shown in Fig. 4(a), all samples exhibited typical type IV isotherms with evident H4 hysteresis loops at relative pressures of 0.4–0.9, which are related to capillary condensation in mesopores [49,50]. The pore size distributions were centered at approximately 3–5 nm. The results in Table 2 show that the pretreatment using H_2O_2 activated the MC since the surface area and total pore volume of the pretreated MC were higher than MC. Moreover, the surface area and total pore volume of $\text{Mo}_2\text{C}/\text{MC}$ were much smaller than those of the pretreated MC support, which was ascribed to carbon atom emission during CHR and Mo_2C nanoparticles blocking a fraction of the carbon pores [51,52]. Interestingly, the surface area and pore volume of the catalysts decreased greatly after nitrogen doping, as shown in Table 2, which might be related to the doped nitrogen causing the mesoporous channels to transform or collapse [53]. In addition, nitrogen doping slightly enlarged the mean pore size from 4.2 nm to 4.4 nm.

H_2 -TPR revealed the reduction process of the molybdenum precursor (Fig. 5). A weak peak at low temperatures and a broad peak at high temperatures were obtained in the TPR profiles. The formation of Mo_2C included three stages: decomposition of the molybdenum precursor into MoO_3 ; reduction of MoO_3 by hydrogen into MoO_2 ; and reduction of MoO_2 by hydrogen and carbon atoms into Mo_2C [54]. As shown in Fig. 5 the first small peak due to the first stage became more intense and shifted to lower temperatures after nitrogen doping, showing that nitrogen facilitated the decomposition of the precursor [55]. The broad peak centered at 350–780 °C was due to the reduction of MoO_3 into MoO_2 and further reduction into Mo_2C . The peak also shifted from 547.2 °C to 545.9 °C and 533.7 °C as the nitrogen dosage increased to 0.5 g and 1.0 g, which indicated that the electron-donating

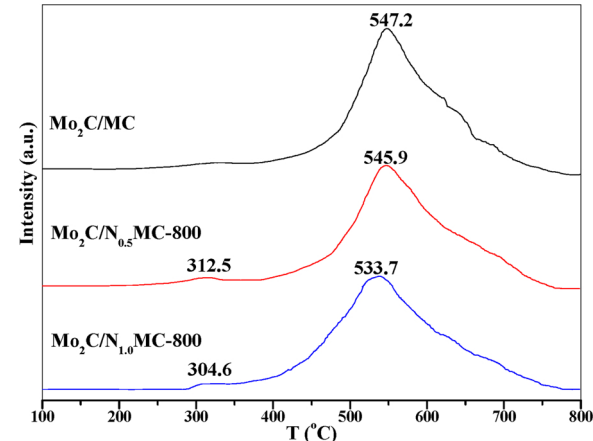


Fig. 5. H_2 -TPR spectra of molybdenum precursor of $\text{Mo}_2\text{C}/\text{MC}$, $\text{Mo}_2\text{C}/\text{N}_{0.5}\text{MC-800}$, and $\text{Mo}_2\text{C}/\text{N}_{1.0}\text{MC-800}$.

effect of nitrogen in the carbon support promoted the reduction of Mo compounds [19,56].

3.2. Hydrotreatment of oleic acid

3.2.1. The catalytic activity of the $\text{Mo}_2\text{C}/\text{NMC}$ catalyst

The results for catalytic hydrotreatment of unsaturated oleic acid over different catalysts are listed in Table 3. For comparison the reaction over pretreated MC was performed, and only a 55.7% conversion and 21.2% selectivity were achieved. The hydrotreatment reaction over $\text{Mo}_2\text{C}/\text{MC}$ attained an 84.8% conversion and 70.1% selectivity, which are higher than those obtained with a commercial Pt/C catalyst (79.8% and 69.1%, respectively), demonstrating the excellent catalytic activity of the Mo_2C catalysts, which was agreed with previous studies [15]. Moreover, the significant difference in the HDO/DC ratio (8.7 vs. 0.1) between both catalysts demonstrated that Mo_2C and the noble catalyst preferred the HDO route and DCX or DCN routes, respectively [17,57]. The hydrotreatment reaction over $\text{Mo}_2\text{C}/\text{N}_{0.5}\text{MC-800}$, $\text{Mo}_2\text{C}/\text{N}_{1.0}\text{MC-800}$, and $\text{Mo}_2\text{C}/\text{N}_{1.5}\text{MC-800}$ attained conversions of 86.2, 90.9, and 91.0% and selectivities of 75.0, 83.3, and 83.4%, respectively, indicating the large improvement in the catalytic activity after doping with nitrogen. This improvement can be mainly attributed to the reduced nanoparticle size and the increased dispersion of Mo_2C (Fig. 3 and Table 2). In addition, the HDO/DC ratio was enhanced from 8.5 to 9.1, 14.0, and 13.4 with the increase in nitrogen. This result may be related to an increase in the local electron density after nitrogen doping changed the ionic character of the catalyst and the adsorption position of the fatty acids onto the catalysts, thus altering the routes of

Table 3

Hydrotreatment of oleic acid over various catalysts.

Entry	Catalyst	Conversion(%)	Selectivity(%)	HDO/DC ratio	Cracking ratio(%)
1	Mo ₂ C/MC	84.8 ± 1.13	70.1 ± 1.31	8.5 ± 0.35	5.5 ± 0.14
2	Mo ₂ C/N _{0.5} MC-800	86.2 ± 1.47	75.0 ± 1.50	9.1 ± 0.51	5.6 ± 0.20
3	Mo ₂ C/N _{1.0} MC-800	90.9 ± 1.53	83.3 ± 1.96	14.0 ± 0.43	5.8 ± 0.17
4	Mo ₂ C/N _{1.5} MC-800	91.0 ± 1.49	83.4 ± 1.22	13.4 ± 0.62	6.7 ± 0.09
5	Pretreated MC	55.7 ± 2.35	21.2 ± 1.80	0.1 ± 0.04	3.5 ± 0.13
6	Pt/C	79.8 ± 1.96	69.1 ± 2.10	0.1 ± 0.02	2.6 ± 0.19
7	Mo ₂ C/N _{1.0} MC-800 ^a	83.7 ± 2.01	67.2 ± 1.97	7.3 ± 0.57	5.2 ± 0.24
8	Mo ₂ C/N _{1.0} MC-800 ^b	75.9 ± 1.87	52.2 ± 1.64	7.2 ± 0.39	4.2 ± 0.15

Reaction condition: catalysts, 1.0 g; oleic acid, 10.0 g; n-hexane (solvent), 50.0 g; initial H₂ pressure, 3.0 MPa; temperature, 350 °C; time, 3 h.^a Melamine as the nitrogen source.^b Aniline as the nitrogen source without polymerization.

hydrotreatment [4]. The melamine and aniline (without polymerization) nitrogen sources did not improve the catalytic activity of the catalysts; however, in contrast, the conversion and selectivity decreased, especially with aniline (entries 7 and 8), which indicated that nitrogen doping with melamine and aniline by direct impregnation is not the proper method for the preparation of Mo₂C/NMC.

The effect of the N_{1.0}MC pyrolysis temperature on the properties and catalytic activity of Mo₂C/N_{1.0}MC were studied, and the results are shown in Table 4. When the pyrolysis temperature increased from 700 °C to 900 °C, the Mo₂C particle size increased from 3.2 nm to 3.9 and 6.3 nm, while the nitrogen content decreased from 2.75 to 2.22 wt %. The nanoparticle size does not simply depend on the nitrogen content because N_{1.0}MC-800 and N_{1.0}MC-900 have similar nitrogen content but the particles sizes were totally different, as shown in Table 4. In section 3.1, the amount of N-6 and N-5 played a leading role in the dispersion of metal ions and metal particles. The total proportion of N-6 and N-5 on N_{1.0}MC-900 was 76.2%, which was much less than that on N_{1.0}MC-800 (86.1%) and N_{1.0}MC-700 (83.4%), explaining the formation of larger particles [29,58]. In addition, the Mo₂C ratio and surface area of the catalysts decreased obviously as the pyrolysis temperature increased. The oleic acid hydrotreatment results showed that the catalytic performance decreased with the increase in the pyrolysis temperature, as indicated by the drop in the conversion from 92.7% to 90.9 and 86.8% and the selectivity greatly decreased from 86.7% to 83.3 and 74.9%. Mo₂C/N_{1.0}MC-700 exhibited the best activity due to the fine particle size of Mo₂C, the high Mo₂C ratio and the high surface area.

The influence of Mo loading on the catalytic hydrotreatment of oleic acid is displayed in Table 5. The conversion and selectivity improved from 81.6% to 92.7% and from 62.5% to 86.7%, respectively, when the Mo loading increased from 10 wt% to 25 wt%, but a further increase in the Mo loading generated an opposite trend for the conversion and selectivity. A similar result pattern was also obtained in our previous research on Mo₂C/MC [16]. The N₂ sorption results in Table 5 reveal that the surface area decreased greatly with the increase in Mo loading, because of the presence of the superfluous Mo. The CO chemical adsorption of catalysts with various Mo loadings was also conducted. Mo dispersion decreased from 2.11% to 0.55% with the increase in the Mo

loading from 10 wt% to 30 wt% as shown in Table 5. In addition, the CO quantity exhibited a similar trend with conversion and selectivity as the Mo loading was varied. The highest CO quantity, 29.58 μmol/g_{cat}, was achieved for 25 wt% Mo loading, which indicated that the number of exposed active sites on the surface of Mo₂C/N_{1.0}MC-700 with 25 wt% Mo loading was the highest, accounting for its optimal catalytic performance. Mo₂C/N_{1.0}MC-700 with 25 wt% Mo loading was chosen for the following research.

To obtain intrinsic insight into the influence of nitrogen doping, the kinetics of the stearic acid hydrotreatment over Mo₂C/N_{1.0}MC-700 and Mo₂C/MC were compared at reaction temperatures of 270, 290, and 310 °C. As shown in Fig. 6(a), the hydrotreatment of the stearic acid over both catalysts obeyed first-order kinetic reaction equation, and the rate constant k, could be calculated from the linear slope of ln(C₀/C_t) versus t. The k values at different temperatures over both catalysts were listed in Table 6. For both catalysts, the k value increased as the reaction temperature increased (for Mo₂C/N_{1.0}MC-700 from 3.52 × 10⁻⁵ to 7.48 × 10⁻⁵ s⁻¹; for Mo₂C/MC from 1.56 × 10⁻⁵ to 4.78 × 10⁻⁵ s⁻¹). As expected, the k values over Mo₂C/N_{1.0}MC-700 were much higher than those over Mo₂C/MC. Notably, the k value over Mo₂C/N_{1.0}MC-700 at 270 °C was 3.52 × 10⁻⁵ s⁻¹, even higher than Mo₂C/MC at 290 °C (2.75 × 10⁻⁵ s⁻¹). Based on the Arrhenius equation, the apparent activation energies and pre-exponential factors for the hydrotreatment of stearic acid over both catalysts were calculated and the results were shown in Table 6. The activation energy over Mo₂C/N_{1.0}MC-700 was 49.7 kJ/mol, which was lower than that of Mo₂C/MC (73.9 kJ/mol). As discussed above, nitrogen doping decreased the particle size of active sites and improved dispersion of Mo, and thus greatly reduced the reaction activation energy and improved catalytic performance. Moreover, the activation energy for the hydrotreatment of stearic acid over Mo₂C/N_{1.0}MC-700 was even lower than that of carbon nanofiber supported Mo₂C in the study of Stellwagen et al. (60 kJ/mol) and of γ-Al₂O₃ supported Ni in the study of Kumar et al. (205.2 kJ/mol) [59,60].

3.2.2. The stability of the Mo₂C/N_{1.0}MC-700 catalyst

The stability of the Mo₂C/N_{1.0}MC-700 catalyst for oleic acid hydrotreatment was investigated, and the results are shown in Fig. 7. After

Table 4The influence of N_{1.0}MC pyrolysis temperature on the properties and catalytic performance of Mo₂C/N_{1.0}MC.

Pyrolysis temp.(°C)	N-6 ^a (%)	N-5 ^a (%)	N-X ^a (%)	Mo(II) ^a (%)	N content ^b (wt%)	d _{TEM} ^c (nm)	S _{BET} ^d (m ² ·g ⁻¹)	Conversion (%)	Selectivity (%)
700	27.5	55.9	16.6	53.1	2.75	3.2 ± 0.9	434	92.7 ± 1.47	86.7 ± 1.74
800	34.1	52.0	13.9	48.8	2.17	3.9 ± 1.1	379	90.9 ± 1.53	83.3 ± 1.96
900	21.4	54.8	23.8	44.0	2.22	6.3 ± 1.1	347	86.8 ± 2.07	74.9 ± 2.15

Reaction condition: catalysts, 1.0 g; oleic acid, 10.0 g; n-hexane (solvent), 50.0 g; initial H₂ pressure, 3.0 MPa; temperature, 350 °C; time, 3 h.^a Detected by XPS analysis.^b Determined by elemental analysis (N_{1.0}MC support).^c Measured by TEM images (more than 200 particles).^d Identified by N₂ sorption.

Table 5Effect of the loading content of Mo on the catalytic performance of $\text{Mo}_2\text{C}/\text{N}_{1.0}\text{MC-700}$.

Loading content ^a (wt%)	Conversion (%)	Selectivity (%)	HDO/DC ratio	Cracking ratio(%)	CO quantity ^b ($\mu\text{mol/g}_{\text{cat}}$)	Dispersion ^b (%)	$S_{\text{BET}}^{\text{c}}$ (m^2g^{-1})
10	81.6 \pm 1.53	62.5 \pm 1.83	6.3 \pm 0.61	4.6 \pm 0.20	23.28	2.11	573.8
15	83.7 \pm 1.11	67.8 \pm 1.69	10.2 \pm 0.46	4.5 \pm 0.14	23.81	2.05	520.8
20	88.9 \pm 2.04	78.9 \pm 2.06	9.9 \pm 0.47	5.6 \pm 0.26	24.36	1.36	474.7
25	92.7 \pm 1.47	86.7 \pm 1.74	13.5 \pm 0.36	6.6 \pm 0.19	29.58	1.19	409.8
30	91.6 \pm 1.59	84.8 \pm 1.58	12.0 \pm 0.31	5.4 \pm 0.17	15.84	0.55	379.2

Reaction condition: catalysts, 1.0 g; oleic acid, 10.0 g; n-hexane (solvent), 50.0 g; initial H_2 pressure, 3.0 MPa; temperature, 350 °C; time, 3 h.^a The practical loading content was analyzed by ICP.^b Detected by CO chemical adsorption.^c Identified by N_2 sorption.

recycling three times, the conversion and selectivity of the catalyst decreased by 4.4% (from 92.7 to 88.3%) and 6.9% (from 86.7 to 79.8%), respectively. Compared with the Mo_2C supported on carbon nanofiber [17] and the Mo_2C supported on activated carbon (25 wt% Mo loading) in our previous study [14], the $\text{Mo}_2\text{C}/\text{N}_{1.0}\text{MC-700}$ catalyst in this study exhibited excellent stability during the oleic acid hydro-treatment, which was likely attributable to strong interactions between the support and active sites due to nitrogen doping. Moreover, the HDO/DC ratio decreased from 13.5 to 10.7 and the cracking ratio was reduced from 6.6% to 4.6% after the catalyst was recycled three times. This could be attributed to the fact that the coke from the unsaturated feed covered some active sites and thus changed the catalytic characteristics of the $\text{Mo}_2\text{C}/\text{N}_{1.0}\text{MC-700}$ catalyst.

To investigate the reasons for catalyst deactivation, the XPS, XRD, and N_2 -sorption of $\text{Mo}_2\text{C}/\text{N}_{1.0}\text{MC-700}$ catalyst after it had been recycled three times were performed and the results were shown in the Supplementary information (Figs. S3–S5). Prior to measurements, the spent catalysts were washed with hexane and methanol three times and dried at 40 °C under a vacuum. The XPS pattern of used the catalyst was similar to that of the fresh catalyst, as exhibited in Fig. S3(a) and (b), manifesting that the Mo_2C (Mo^{2+}) remained after recycling it three times. This result was consistent with XRD analysis in Fig. S4. In addition, in the XRD spectrum of the used catalyst the broad peaks at 24°, representing the (002) plane of the graphite structure, became more intense compared to that of the fresh catalyst. This indicated that there was possible coke deposition on the surface of the used catalyst, and the nitrogen sorption was further conducted to verify this hypothesis. The nitrogen sorption results in Fig. S5 revealed that the surface area and pore volume decreased drastically from 434 to 88 m^2g^{-1} and from 0.302 to 0.09 cm^3g^{-1} respectively. The adsorption-desorption isotherms did not close, showing that N_2 was desorbed deficiently, as evidence of the solid swelling. This result is similar to our previous study on used molybdenum carbide supported on activated carbon [14]. The

unsaturated feed is thought to form coke, which deposits on the surface of the catalysts and alters the textural structure of the catalyst, thus leading to deactivation [61].

3.2.3. Oleic acid hydro-treatment conditions

In this part the oleic acid hydro-treatment parameters, including the reaction temperature, initial H_2 pressure, as well as the solvents, were investigated, and the results are shown in Fig. 8. To study the influence of the reaction temperature on the catalytic performance, oleic acid hydro-treatments were conducted at 320, 330, 340, 350 and 360 °C. As the reaction temperature increased, the conversion and selectivity increased from 78.8 to 93.5% and from 60.0 to 87.3%, respectively, showing that high temperatures accelerated the oleic acid hydro-treatment. Notably, the HDO/DC ratio improved from 10.6 to 16.2 with the increase in temperature from 320 to 340 °C; however, a further increase in temperature caused a reduction in the HDO/DC ratio. A high reaction temperature promotes the DC routes that were proved in previous studies [62]. Meanwhile, the temperature increase enhanced the cracking ratio and thus improved the content of light alkanes (C9 to C14) from 2.2 to 8.7%. The high temperature appeared to promote breakage of carbon-carbon bond and the cracking reaction is undesired in the hydro-treatment reaction because of the loss of carbon. Considering the high catalytic activity and low cracking reaction at 350 °C, this temperature was regarded as the optimal reaction temperature.

Fig. 8(b) shows the effect of the initial H_2 pressure (1.5 to 3.5 MPa) on the hydro-treatment of oleic acid. Among the three hydro-treatment pathways, the hydrogen consumption was greatest in the HDO route in which the mole ratio of oleic acid/hydrogen was 1:3. In the hydro-treatment reaction of oleic acid, the theoretical consumption of hydrogen by HDO was 0.96 MPa, and therefore, the initial hydrogen provided in this study was sufficient. As the initial H_2 pressure increased from 1.5 to 3.5 MPa, the conversion and selectivity significantly increased from 82.3 to 92.6% and from 65.0 to 85.7%, respectively,

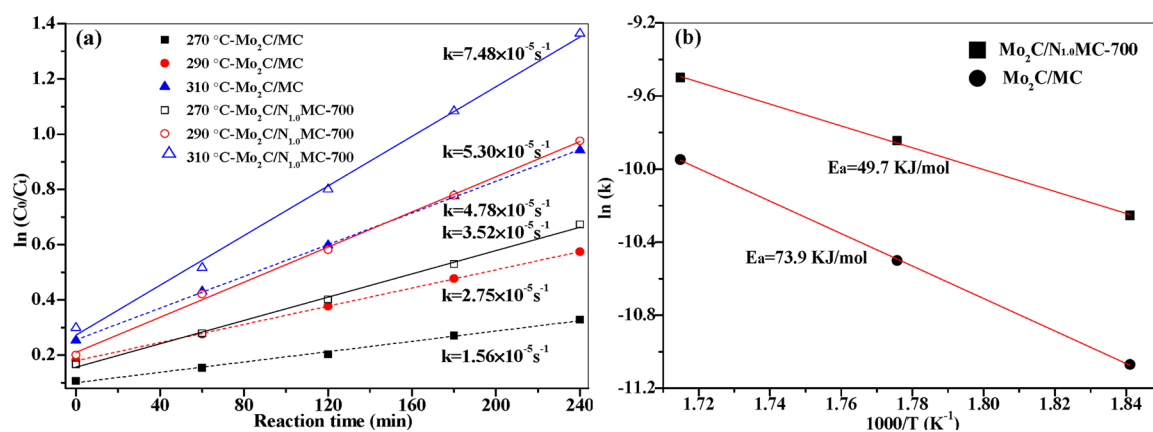


Fig. 6. Catalytic activity (a) and Arrhenius plots (b) for stearic acid hydro-treatment over $\text{Mo}_2\text{C}/\text{N}_{1.0}\text{MC-700}$ and $\text{Mo}_2\text{C}/\text{MC}$ catalysts. Reaction condition: catalyst, 0.25 g; stearic acid, 5.0 g; n-hexane (solvent), 100.0 g; initial H_2 pressure, 3.0 MPa; temperature, 270–310 °C; time, 0–4 h.

Table 6Activation energy values and pre-exponential factors for stearic acid hydrotreatment over $\text{Mo}_2\text{C}/\text{N}_{1.0}\text{MC-700}$ and $\text{Mo}_2\text{C}/\text{MC}$ catalysts.

k (s^{-1})	Reaction temperature (K)			Arrhenius parameters		
	543.15	563.15	583.15	E_a (kJ/mol)	A (s^{-1})	R^2
$\text{Mo}_2\text{C}/\text{N}_{1.0}\text{MC-700}$	3.52×10^{-5}	5.30×10^{-5}	7.48×10^{-5}	49.7	198.62	0.998
$\text{Mo}_2\text{C}/\text{MC}$	1.56×10^{-5}	2.75×10^{-5}	4.78×10^{-5}	73.9	2.15	0.999

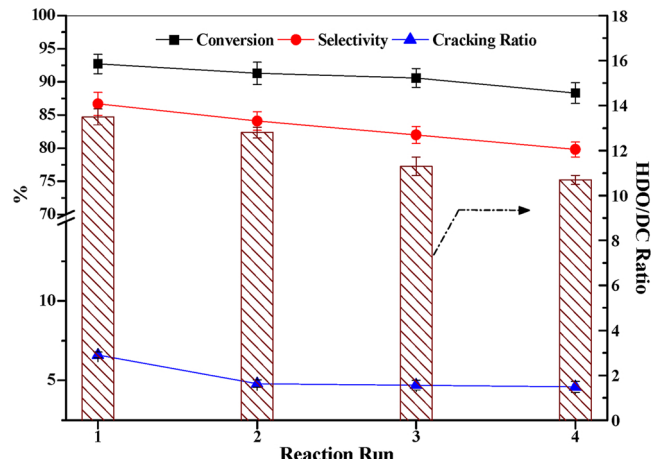


Fig. 7. Recyclability of $\text{Mo}_2\text{C}/\text{N}_{1.0}\text{MC-700}$ with 25 wt% for the hydrotreatment of oleic acid. Reaction condition: catalysts, 1.0 g; oleic acid, 10.0 g; n-hexane (solvent), 50.0 g; initial H_2 pressure, 3.0 MPa; temperature, 350 °C; time, 3 h.

showing that a high initial H_2 pressure was favorable for the hydrotreatment reaction. Moreover, the HDO/DC ratio was greatly improved, while the cracking ratio rarely varied with the increase in the initial H_2 pressure.

To study the influence of the solvent on the hydrotreatment of oleic acid, n-hexane, n-heptane, n-octane, and cyclohexane were used as solvents. Table 7 reveals that catalytic performance decreased in the following order: n-hexane > n-heptane > n-octane > cyclohexane (entries 1–4). When straight-chain alkanes were used as solvents in the hydrotreatment reaction, the catalytic activity was closely related to the carbon number of the solvent. The poor catalytic performance of cyclohexane demonstrated that cyclohexane was unsuitable as a solvent in this reaction compared with a straight-chain alkane with the same number of carbons. Moreover, the HDO/DC ratio in cyclohexane was much lower than that in straight-chain alkanes, showing that cyclohexane restrained the HDO pathway during the hydrotreatment of oleic

acid. The supercritical temperatures of n-hexane, n-heptane, n-octane, and cyclohexane were 234, 267, 296, and 280 °C, respectively. At a 350 °C reaction temperature the four solvents exist in the form of a supercritical fluid, in which the high diffusivity can reduce the mass transfer resistance, causing more contact between the catalyst and the reactants [15]. The higher supercritical temperature of n-octane and cyclohexane explain the poor catalytic performance of $\text{Mo}_2\text{C}/\text{N}_{1.0}\text{MC-700}$ catalyst in both solvents.

3.2.4. Hydrotreatment of different feedstocks and reaction scheme

To study the difference among feedstocks during the reaction, the hydrotreatments of unsaturated oleic acid, methyl oleate, saturated stearic acid, and methyl stearate were conducted and the results are listed in Table 7 (entries 5–8). The conversion of the four substrates was high (above 91%), but the selectivity decreased in the following order: methyl stearate (92.5%), stearic acid (89.5%), methyl oleate (87.9%), and oleic acid (86.7%). The $\text{Mo}_2\text{C}/\text{N}_{1.0}\text{MC-700}$ catalyst exhibited higher catalytic activity for the saturated feedstock than the unsaturated feedstock (stearic acid vs. oleic acid; methyl stearate vs. methyl oleate). During the hydrotreatment of the unsaturated substrate, the first step is the formation of a saturated fatty acid or FAME by hydrogenation. Nevertheless, it cannot explain the higher catalytic activity for the saturated feedstock than unsaturated feedstock because the hydrogenation rate was extremely rapid. According to previous studies, the unsaturated feedstock is prone to a coke reaction that reduces the catalytic activity [17,61]. The catalytic performance of the fatty acids was lower than that of FAME, revealing that the fatty acids are not the prominent intermediates of FAME. The same results were found in other studies [15,61].

In order to study the FAME hydrotreatment pathway, the experiment with low conversion was carried out at 350 °C for 1 h to observe intermediates. In addition to the saturated FAME and a trace amount of fatty acid, the aldehyde, 1-alcohol, and 1-olefin with the same carbon number as the fatty acid were also detected. However, the enol was not found because of its instability. Based on these intermediates and related reports [1,4,63], the proposed mechanism of the hydrotreatment of unsaturated FAME over $\text{Mo}_2\text{C}/\text{N}_{1.0}\text{MC-700}$ is outlined in Scheme 2.

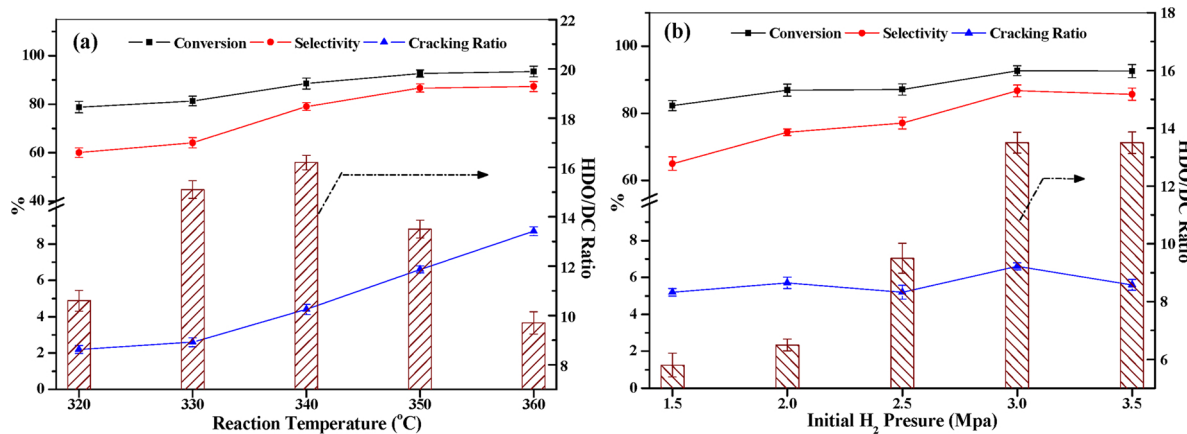
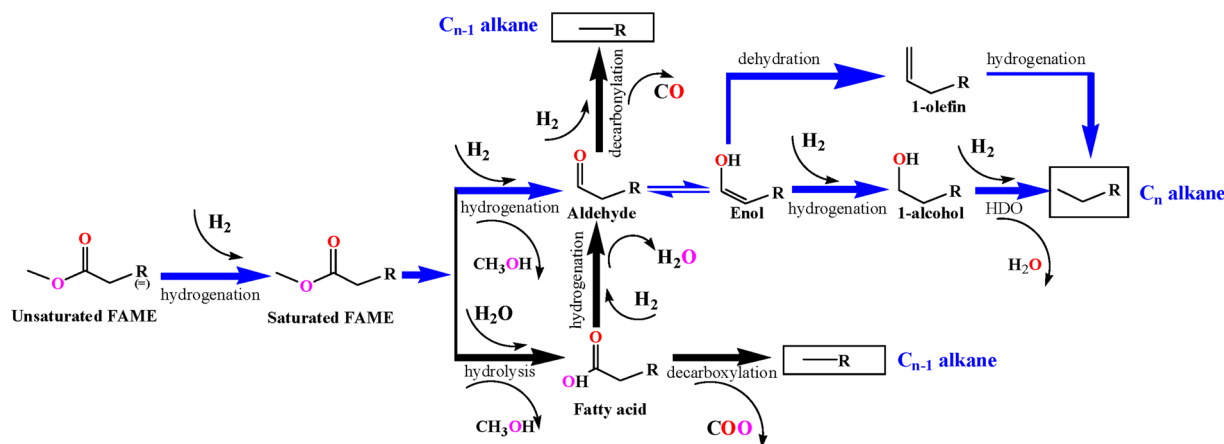


Fig. 8. Effects of (a) reaction temperature (initial H_2 pressure: 3.0 MPa) and (b) initial H_2 pressure (reaction temperature: 350 °C) on the hydrotreatment of fatty acids. Other reaction condition: n-hexane (solvent), 50.0 g; oleic acid, 10.0 g; $\text{Mo}_2\text{C}/\text{N}_{1.0}\text{MC-700}$, 1.0 g; time, 3 h.

Table 7

The effect of solvent and feedstock on catalytic hydrotreatment.

Entry	Solvent/Substrate	Conversion(%)	Selectivity(%)	HDO/DC ratio	Cracking ratio(%)
1	n-hexane ^a	92.7 ± 1.47	86.7 ± 1.74	13.5 ± 0.36	6.6 ± 0.19
2	n-heptane ^a	91.6 ± 1.67	84.9 ± 1.30	13.4 ± 0.44	5.4 ± 0.25
3	n-octane ^a	87.3 ± 1.81	75.4 ± 1.59	15.5 ± 0.29	3.9 ± 0.18
4	cyclohexane ^a	85.3 ± 2.03	72.0 ± 1.60	9.3 ± 0.27	5.1 ± 0.21
5	oleic acid ^b	92.7 ± 1.47	86.7 ± 1.74	13.5 ± 0.36	6.6 ± 0.19
6	stearic acid ^b	91.7 ± 1.94	89.5 ± 2.05	16.1 ± 0.40	1.7 ± 0.17
7	methyl oleate ^b	92.9 ± 1.22	87.9 ± 1.14	12.6 ± 0.19	6.1 ± 0.16
8	methyl stearate ^b	94.2 ± 1.87	92.5 ± 2.38	29.5 ± 0.45	1.4 ± 0.23

Reaction condition: temperature: 350 °C; initial H₂ pressure: 3.0 MPa; Mo₂C/N_{1.0}MC-700, 1.0 g; time, 3 h.^a Substrate, oleic acid 10.0 g.^b Solvent, n-hexane 50.0 g.**Scheme 2.** The reaction process of FAME hydrotreatment over Mo₂C/N_{1.0}MC-700. blue arrow: main reactions; R(=): unsaturated C14 or C16.

The first step is the saturation of the carbon double bond and its reaction rate is very fast. Afterwards, the saturated FAME is predominantly hydrogenated into aldehydes rather than hydrolyzed into fatty acids because fatty acids can not be generated from FAME through a β -elimination step [64,65]. A trace amount fatty acid in product is supposed from FAME via hydrolysis since the H₂O could be formed in other pathways. The fatty acids is either converted by DCX into C_{n-1} alkanes of one carbon atom shorter, or by hydrogenation into aldehydes. The conversion of aldehydes has two possible reaction paths: DCN to form C_{n-1} alkanes or transformation to its enol form. The 1-olefin from the dehydration of the enol by hydrogenation generated the C_n alkanes, which has the same carbon chain length as the fatty acids. The other pathway that produced C_n alkanes from enol is the formation of saturated alcohols through hydrogenation followed by dehydration and hydrogenation.

4. Conclusion

Nitrogen-doped mesoporous carbon (NMC) was synthesized by the in situ polymerization of aniline on the surface of MC followed by pyrolysis. Afterwards, the NMC supported Mo₂C catalyst was prepared for fatty acids and FAME hydrotreatment. XPS and elemental analysis results revealed that nitrogen was successfully doped into the carbon skeleton, mainly in the form of pyridinic N and pyrrolic N, which played an important role in anchoring the active sites and enhancing metal dispersion. Doped nitrogen reduced the Mo₂C particle size and improved the dispersion of Mo, as shown by the TEM and CO chemical adsorption results. In the oleic acid hydrotreatment, the conversion and selectivity over the best catalyst (Mo₂C/N_{1.0}MC-700 with 25 wt% Mo loading) were 92.7% and 86.7% respectively, which are much higher than those obtained over Mo₂C/MC (84.8% and 70.1%). The kinetic

study showed that the apparent activation energy for the hydrotreatment of stearic acid over Mo₂C/N_{1.0}MC-700 was 49.7 kJ/mol, which was lower than that of Mo₂C/MC (73.9 kJ/mol). Moreover, after recycling three times, the conversion and selectivity over Mo₂C/N_{1.0}MC-700 decreased by 4.4% and 6.9%, respectively. The deactivation was mainly ascribed to the coke deposition on the surface of catalyst. The high catalytic performance and stability of the catalyst were ascribed to the particle size reduction, increase in dispersion and the enhanced interactions between the support and active sites due to nitrogen doping. The hydrotreatment condition were also optimized as follows: reaction temperature, 350 °C; initial H₂ pressure, 3.0 MPa; and n-hexane as the solvent. Moreover, the study showed that feedstocks with saturated carbon-carbon bonds and ester groups were more easily converted into hydrocarbons.

Acknowledgements

This work was supported financially by the Key Technology for Preparing Aviation Fuel by Controlled Hierarchical Evolution of Woody Oil [grant numbers CAFYBB2017ZC004] and the National Natural Science Foundation of China [grant numbers 31770612]. The authors would like to thank Weihong Tan (ICIFP) for her help with the measurement of GC-MS, Hongxiao Wang (ICIFP) for his help with the XRD and TEM, Haitao Huang (ICIFP) for his help with the N₂ sorption, Juanzhang Shen (ICIFP) for her help with the ICP and elemental analysis, and Xiangxiang Gong (Testing Center of Yangzhou University) for his help with the XPS. The authors would also like to thank Dr. Gangli Zhu (Chinese Academy of Sciences), Dr. Yunwu Zheng (Southwest Forestry University), and Dr. Yue Du (Wu Han University of Technology) for their suggestions on the kinetic study.

Appendix A. Supplementary data

Supplementary material related to this article can be found, in the online version, at doi:<https://doi.org/10.1016/j.apcatb.2018.09.077>.

References

- [1] A.E. Coumans, E.J.M. Hensen, *Appl. Catal. B: Environ.* 201 (2017) 290–301.
- [2] E.-M. Ryymä, M.L. Honkela, T.-R. Viljava, A.O.I. Krause, *Appl. Catal. A: Gen.* 358 (2009) 42–48.
- [3] E. Kordouli, B. Pawelec, K. Bourikas, C. Kordulis, J.L.G. Fierro, A. Lycourghiotis, *Appl. Catal. B: Environ.* 229 (2018) 139–154.
- [4] R.W. Gosselink, S.A. Hollak, S.W. Chang, J. van Haveren, K.P. de Jong, J.H. Bitter, D.S. van Es, *ChemSusChem* 6 (2013) 1576–1594.
- [5] L.N. Silva, I.C.P. Fortes, F.P. de Sousa, V.M.D. Pasa, *Fuel* 164 (2016) 329–338.
- [6] L. Zhou, A. Lawal, *Appl. Catal. A Gen.* 532 (2017) 40–49.
- [7] N.A. Grossi-Giordano, T.R. Eaton, Z. Bo, S. Yacob, C.-C. Yang, J.M. Notestein, *Appl. Catal. B* 192 (2016) 93–100.
- [8] N. Chen, N. Wang, Y. Ren, H. Tominaga, E.W. Qian, *J. Catal.* 345 (2017) 124–134.
- [9] Y. Shao, Q. Xia, X. Liu, G. Lu, Y. Wang, *ChemSusChem* 8 (2015) 1761–1767.
- [10] D. Kubíčka, J. Horáček, M. Setnička, R. Bulánek, A. Zukal, I. Kubíčková, *Appl. Catal. B: Environ.* 145 (2014) 101–107.
- [11] P. Arora, H. Ojagh, J. Woo, E. Lind Grennfelt, L. Olsson, D. Creaser, *Appl. Catal. B: Environ.* 227 (2018) 240–251.
- [12] S.K. Kim, D. Yoon, S.-C. Lee, J. Kim, *ACS Catal.* 5 (2015) 3292–3303.
- [13] M.M. Sullivan, C.-J. Chen, A. Bhan, *Catal. Sci. Technol.* 6 (2016) 602–616.
- [14] F. Wang, J. Xu, J. Jiang, P. Liu, F. Li, J. Ye, M. Zhou, *Fuel* 216 (2018) 738–746.
- [15] J. Han, J. Duan, P. Chen, H. Lou, X. Zheng, H. Hong, *Green Chem.* 13 (2011) 2561–2568.
- [16] F. Wang, J. Jiang, K. Wang, Q. Zhai, H. Sun, P. Liu, J. Feng, H. Xia, J. Ye, Z. Li, F. Li, J. Xu, *Fuel* 228 (2018) 103–111.
- [17] S.A.W. Hollak, R.W. Gosselink, D.S. van Es, J.H. Bitter, *ACS Catal.* 3 (2013) 2837–2844.
- [18] S. Jing, L. Zhang, L. Luo, J. Lu, S. Yin, P.K. Shen, P. Tsiakaras, *Appl. Catal. B: Environ.* 224 (2018) 533–540.
- [19] R. Nie, H. Yang, H. Zhang, X. Yu, X. Lu, D. Zhou, Q. Xia, *Green Chem.* 19 (2017) 3126–3134.
- [20] J. Xia, G. He, L. Zhang, X. Sun, X. Wang, *Appl. Catal. B: Environ.* 180 (2016) 408–415.
- [21] T. Cordero-Lanzac, R. Palos, J.M. Arandes, P. Castaño, J. Rodríguez-Mirasol, T. Cordero, J. Bilbao, *Appl. Catal. B: Environ.* 203 (2017) 389–399.
- [22] R. Nie, M. Miao, W. Du, J. Shi, Y. Liu, Z. Hou, *Appl. Catal. B: Environ.* 180 (2016) 607–613.
- [23] E. Haque, J.W. Jun, S.N. Talapaneni, A. Vinu, S.H. Jhung, *J. Mater. Chem.* 20 (2010) 10801.
- [24] Z. Wei, J. Wang, S. Mao, D. Su, H. Jin, Y. Wang, F. Xu, H. Li, Y. Wang, *ACS Catal.* 5 (2015) 4783–4789.
- [25] J. Li, S. Wang, H.-Y. Liu, H.-J. Zhou, Y. Fu, *ChemistrySelect* 2 (2017) 33–41.
- [26] X. Cui, A.E. Surkus, K. Junge, C. Topf, J. Radnik, C. Kreyenschulte, M. Beller, *Nat. Commun.* 7 (2016) 11326.
- [27] X. Xu, Y. Li, Y. Gong, P. Zhang, H. Li, Y. Wang, *J. Am. Chem. Soc.* 134 (2012) 16987–16990.
- [28] R. Liu, S.M. Mahurin, C. Li, R.R. Unocic, J.C. Idrobo, H. Gao, S.J. Pennycook, S. Dai, *Angew. Chem.* 50 (2011) 6799–6802.
- [29] Y. Liu, X. Yang, H. Liu, Y. Ye, Z. Wei, *Appl. Catal. B: Environ.* 218 (2017) 679–689.
- [30] J. Han, J. Duan, P. Chen, H. Lou, X. Zheng, H. Hong, *ChemSusChem* 5 (2012) 727–733.
- [31] T. Mo, J. Xu, Y. Yang, Y. Li, *Catal. Today* 261 (2016) 101–115.
- [32] L.A. Sousa, J.L. Zötin, V. Teixeira da Silva, *Appl. Catal. A: Gen.* 449 (2012) 105–111.
- [33] X. Li, K. Tie, Z. Li, Y. Guo, Z. Liu, X. Liu, X. Liu, H. Feng, X.S. Zhao, *Appl. Surf. Sci.* 447 (2018) 57–62.
- [34] J. Yu, M. Guo, F. Muhammad, A. Wang, G. Yu, H. Ma, G. Zhu, *Microporous Mesoporous Mater.* 190 (2014) 117–127.
- [35] H. Wang, C. Sun, Y. Cao, J. Zhu, Y. Chen, J. Guo, J. Zhao, Y. Sun, G. Zou, *Carbon* 114 (2017) 628–634.
- [36] E. Ochoa, D. Torres, R. Moreira, J.L. Pinilla, I. Suelves, *Appl. Catal. B: Environ.* 239 (2018) 463–474.
- [37] J.A. Prithi, N. Rajalakshmi, G. Ranga Rao, *Int. J. Hydrogen Energy* 43 (2018) 4716–4725.
- [38] A.-d. Tan, Y.-f. Wang, Z.-y. Fu, P. Tsiakaras, Z.-x. Liang, *Appl. Catal. B: Environ.* 218 (2017) 260–266.
- [39] N. Daems, J. Wouters, C. Van Goethem, K. Baert, C. Poleunis, A. Delcorte, A. Hubin, I.F.J. Vankelecom, P.P. Pescarmona, *Appl. Catal. B: Environ.* 226 (2018) 509–522.
- [40] Z. Yu, X. Wang, Y.-N. Hou, X. Pan, Z. Zhao, J. Qiu, *Carbon* 117 (2017) 376–382.
- [41] T. Lin, I. Chen, F. Liu, C. Yang, H. Bi, F. Xu, F. Huang, *Science* 350 (2015) 1508–1513.
- [42] L. Hu, R. Zhang, L. Wei, F. Zhang, Q. Chen, *Nanoscale* 7 (2015) 450–454.
- [43] J.R. Pels, F. Kapteijn, J.A. Moulijn, Q. Zhu, K.M. Thomas, *Carbon* 33 (1995) 1641–1653.
- [44] S. Gao, H. Fan, X. Wei, L. Li, Y. Bando, D. Golberg, *Part. Part. Syst. Charact.* 30 (2013) 864–872.
- [45] L. Lin, Q. Zhu, A.W. Xu, *J. Am. Chem. Soc.* 136 (2014) 11027–11033.
- [46] R. Shi, J. Zhao, S. Liu, W. Sun, H. Li, P. Hao, Z. Li, J. Ren, *Carbon* 130 (2018) 185–195.
- [47] J. Zhang, L. Ma, M. Gan, F. Yang, S. Fu, X. Li, *J. Power Sources* 288 (2015) 42–52.
- [48] M.V. Morales, E. Asedegbe-Nieto, B. Bachiller-Baeza, A. Guerrero-Ruiz, *Carbon* 102 (2016) 426–436.
- [49] F. Wang, Y. Zheng, Y. Huang, X. Yang, G. Xu, J. Kang, C. Liu, Z. Zheng, *J. Anal. Appl. Pyrolysis* 126 (2017) 180–187.
- [50] Y. Zhao, X. Bo, L. Guo, *Electrochim. Acta* 176 (2015) 1272–1279.
- [51] P. Liang, H. Gao, Z. Yao, R. Jia, Y. Shi, Y. Sun, Q. Fan, H. Wang, *Catal. Sci. Technol.* 7 (2017) 3312–3324.
- [52] C. Liang, P. Ying, C. Li, *Chem. Mater.* 14 (2002) 3148–3151.
- [53] D. Zhang, L. Zheng, Y. Ma, L. Lei, Q. Li, Y. Li, H. Luo, H. Feng, Y. Hao, *ACS Appl. Mater. Interfaces* 6 (2014) 2657–2665.
- [54] C. Liang, W. Ma, Z. Feng, C. Li, *Carbon* 41 (2003) 1833–1839.
- [55] P. Chen, F. Yang, A. Kostka, W. Xia, *ACS Catal.* 4 (2014) 1478–1486.
- [56] G. Zhang, S. Zang, L. Lin, Z.A. Lan, G. Li, X. Wang, *ACS Appl. Mater. Interfaces* 8 (2016) 2287–2296.
- [57] A. Dragu, S. Kinayyigit, E.J. Garcíasuárez, M. Florea, E. Stepan, S. Velea, L. Tanase, V. Collière, K. Philippot, P. Granger, V.I. Parvulescu, *Appl. Catal. A Gen.* 504 (2015) 81–91.
- [58] M. Chen, L.-L. Shao, Y.-P. Liu, T.-Z. Ren, Z.-Y. Yuan, *J. Power Sources* 283 (2015) 305–313.
- [59] D.R. Stellwagen, J.H. Bitter, *Green Chem.* 17 (2015) 582–593.
- [60] P. Kumar, S.R. Yenumala, S.K. Maity, D. Shee, *Appl. Catal. A Gen.* 471 (2014) 28–38.
- [61] M. Snåre, I. Kubíčková, P. Mäki-Arvela, D. Chichova, K. Eränen, D.Y. Murzin, *Fuel* 87 (2008) 933–945.
- [62] C. Miao, O. Marin-Flores, S.D. Davidson, T. Li, T. Dong, D. Gao, Y. Wang, M. García-Pérez, S. Chen, *Fuel* 166 (2016) 302–308.
- [63] Q. Guan, F. Wan, F. Han, Z. Liu, W. Li, *Catal. Today* 259 (2016) 467–473.
- [64] B. Donnis, R.G. Eggeberg, P. Blom, K.G. Knudsen, *Top. Catal.* 52 (2009) 229–240.
- [65] M. Snåre, I. Kubíčková, P. Mäki-Arvela, K. Eränen, J. Wärnå, D.Y. Murzin, *Chem. Eng. J.* 134 (2007) 29–34.